Wielki, Nicole ; Sonnenberg, Heike ; Meyer, Daniel ; Clausen, Brigitte

Particle-oriented peening as method to investigate the material dependent deformation behaviour

Journal Article	as:	peer-reviewed accepted version (Postprint)
DOI of this document*(secondary publication):		https://doi.org/10.26092/elib/3644
Publication date of this document:		07/02/2025

* for better findability or for reliable citation

Recommended Citation (primary publication/Version of Record) incl. DOI:

Nicole Wielki, Heike Sonnenberg, Daniel Meyer, Brigitte Clausen,
Particle-oriented peening as method to investigate the material dependent deformation behaviour,
Journal of Materials Processing Technology, Volume 289, 2021, 116960,
ISSN 0924-0136, https://doi.org/10.1016/j.jmatprotec.2020.116960.

Particle-oriented peening as method to investigate the material dependent deformation behaviour

Nicole Wielki[*, a], Heike Sonnenberg[a], Daniel Meyer[a, b], Brigitte Clausen[a, b]

[a] University of Bremen and MAPEX Center for Materials and Processes, Bibliothekstr. 1, 28359 Bremen; Germany, wielki@iwt-bremen.de, +49 421 218 51132, ORCID: 0000-0002-0327-4037 (N.W.), sonnenberg@iwt-bremen.de, ORCID: 0000-0001-9497-0494 (H.S.), dmeyer@iwt-bremen.de, ORCID: 0000-0003-2747-6589 (D.M.), clausen@iwt-bremen.de, ORCID: 0000-0003-3518-4519 (B.C.)

[b] IWT Leibniz-Institute for Materials Engineering, Badgasteiner Str. 3, 28359 Bremen, Germany

*Correspondence: wielki@iwt-bremen.de, +49 421 218 51132, ORCID: 0000-0002-0327-4037

Graphical abstract

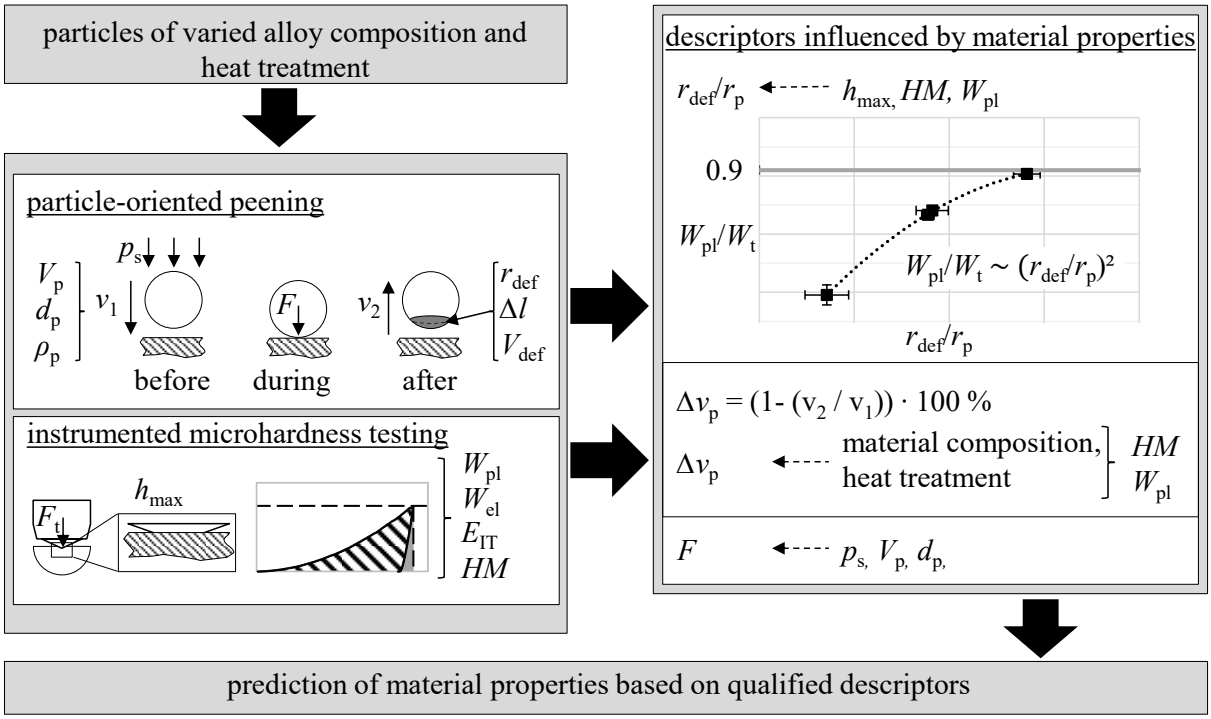

Abstract

The material and its microstructure define the behaviour of a part in a deformation process. A single particle deformation process is introduced as a rapid material characterization method extending already existing approaches. Particle-oriented peening is performed with spherical micro samples of the low carbon steel 100Cr6 (AISI 52100) and the martensitic stainless steel X46Cr13 (AISI 420). Three different diameters (0.6 mm, 0.8 mm and 1.0 mm) were chosen to investigate the impact of the material and the surface to volume ratio. By processing single particles, the mechanical and geometrical properties of the particle before and after the impact can be linked to the deformation behaviour during the peening process. The elastic and plastic

material properties are revealed by studying the remaining plastic deformation of the particle and the velocity reduction as a result of the impact. Instrumented universal micro hardness measurements are carried out to determine the hardness of the particles and to correlate it with the particles' behaviour during the particle-oriented peening process. The plastic deformation work as a characteristic value of micro hardness measurements of the different material states is discussed. It is conceivable that the consideration of different material behaviour related values (so-called descriptors) may replace conventional material testing in the future. Using short-term characterization methods like the particle-oriented peening a fast determination of material properties is possible.

Keywords

Material characterization, particle-oriented peening, plastic deformation, universal micro hardness measurement, shot peening

Nomenclature

a	distance between nozzle and contact plate [mm]
a_p	acceleration of the particle [m/s²]
A_{def}	flattened surface on peened ball or sphere [µm²]
d_p	particle diameter [mm]
F	impact force [N]
F_t	testing force [N]
$F_{t,\,max}$	maximum force [N]
F_z	measured force [N]
H_{IT}	indentation hardness
HM	Martens hardness
h_{max}	indentation depth at maximum testing force [µm]
Δl	linear plastic deformation [µm]
m_p	particle mass [kg]
p	impulse [kg · m/s]
p_s	jet pressure [bar]
R	coefficient of determination [-]
r_p	particle radius [mm]
r_{def}	deformation radius of flattened surface A_{def} [µm]
t	time [s]
t_c	contact time [s]
V_{def}	calculated volume of deformed spherical segment [µm³]
V_p	total volume of the particle [µm³]
v_p, v_1, v_2	particle velocity ($_1$ before (≙ process velocity), $_2$ after the impact) [m/s]
Δv_p	velocity reduction [%]
W_{el}	elastic deformation work [µJ]
W_{pl}	plastic deformation work [µJ]
W_{pl}/W_t	relative plastic deformation work [-]
W_t	total deformation work [µJ]
σ	standard deviation

1 Introduction and motivation

As described by Ellendt and Mädler (2018), the selection of materials for a particular application is load-oriented and strongly driven by requirements such as mechanical properties. The mechanical properties are influenced not only by the material composition but also by the process chain (heat treatment, etc.). Thelning (2013) describes various standardized methods, e.g. tensile or impact tests, to examine and verify the properties of a steel after heat treatment. Each procedure requires a standardized sample geometry of macroscopic size and is carried out using a specific experimental set-up. The test itself and the sample preparation is usually time-consuming. The production of the samples already requires the synthesis of large volumes of the material, which is subsequently subjected to mechanical, thermal or thermomechanical treatments. Consequently, statements about the mechanical properties of materials for e.g. structural elements can only be made after time-, material-, and cost-intensive experimental investigations.

Ellendt and Mädler (2018) propose the method "Farbige Zustände" to enable a fast and resource-efficient analysis of new materials as an alternative to conventional material development and testing. In this method, alternative values that describe the material behaviour (so-called descriptors) are determined on spherical micro samples (diameter less than 1.0 mm) using new and fast testing methods adapted to these micro samples. For high accuracy, the descriptors are determined during or as a result of highly defined processes. To extend the spectrum of alloying composition beyond commercially available micro samples, samples can be generated comparatively quickly in large batches using for example the drop on demand technique. As described by Imani Moqadam et al. (2019), the single droplet generation is triggered by introducing a mechanical or pneumatic momentum into the melt which expels the exact droplet volume. The resulting microstructure of the particles can be influenced within the process e.g. by adjusting the cooling conditions as presented by Ellendt et al. (2016). The high reproducibility of the particles produced by drop on demand is shown in studies by Imani Moqadam et al. (2020). Samples of the materials X210Cr12 (AISI D3) and 41Cr4 (AISI 5140) are investigated using different descriptor-based processes revealing standard deviations within the range of conventional bearing balls.

Zhao (2006) reviews combinatorial approaches for material characterization. He points out that although thin films are commonly used for the determination of properties of functional materials they allow only limited conclusions about the behaviour of the bulk material. Since

the influence of the microstructure can be taken into account for the above mentioned spherical micro samples, Mädler (2014) claims that here, the transferability regarding material properties from the micro to the macro scale is possible.

The applicability of the particle-oriented peening process for characterizing the deformation behaviour of small particles depending on their material was first demonstrated by Kämmler et al. (2019). According to e.g. Schulze (2006) shot peening is conventionally used to beneficially influence the properties of e.g. a contact plate. By utilizing a contact plate with a hardness exceeding the hardness of the particles, shot peened particles can be deformed plastically which is shown by Kämmler et al. (2019). While the contact plate only deforms elastically, at high impact velocities elasto-plastic deformation is obtained for the shot peened particles. The examination of the remaining plastic deformation of the particles revealed differences between the investigated AlSi12 and X210Cr12 (AISI D3) particles. Due to their higher hardness, the latter showed lower plastic deformations when subjected to the same process conditions compared to the significantly softer aluminum particles. Kämmler et al. (2019) used a conventional shot peening setup which accelerated a large number of particles simultaneously. The mutual interaction of the particles could therefore not be avoided and certainly had an influence on the results obtained. A high number of samples was needed and processed simultaneously. Only the approaching velocity and the remaining plastic deformation of particles were analysed and it was accepted that it was not known what impact conditions each exact sample was subjected to.

In the present work, the method of a single particle deformation process, the particle-oriented peening, which was developed subsequently to the investigations of Kämmler et al. (2019) is introduced in detail. This new development enables the investigation of individual particles and offers a basis for future automation in terms of high-throughput. The potential of this process for the characterization of materials has already been shown in the publications of Steinbacher et al. (2019) and Imani Moqadam et al. (2020). Steinbacher et al. (2019) showed the influence of heat treatment on e.g. the plastic deformation and the velocity reduction of 100Cr6 (AISI 52100) bearing balls. Based on these descriptive values a differentiation between the heat treatment states was possible. Furthermore, Imani Moqadam et al. (2020) were able to differentiate between the materials X210Cr12 (AISI D3) and 41Cr4 (AISI 5140) based on descriptor-based investigations. Based on these investigations, correlations between the material hardness and the values obtained in particle-oriented peening are expected. The

sensitivity of the characterization values (descriptors) is analysed by investigating different heat treatments of the same material. The influence of the alloy composition is considered by using two steels with different carbon and chromium contents.

Antonyuk (2006) investigates the deformation and fracture behaviour of spherical granules at compressive stress (low loading rate) and impact stress (high loading rate). Based on his work, the descriptors which describe the deformation until failure can be correlated with material properties like the Young's modulus, the yield strength, the yield stress, the stiffness and the deformation energy. In order to obtain information on the development of the determined descriptors in dependence on the particle size, different particle sizes are considered within the present work. The exceeding of the yield strength due to high pressure in the contact area is geometry-dependent and therefore influenced by the particle size according to Antonyuk (2006). Consequently, an influence of the particle diameter on the descriptors can be assumed. This assumption is supported by investigations of Sonnenberg and Clausen (2018), who have examined particles with diameters of 0.4 mm, 0.6 mm, 0.8 mm, and 1.0 mm of the material X46Cr13 (martensitic microstructure, approx. 60 HRC) in micro compression tests. By adjusting the test force and relating it to the initial diameter, comparable normalized force-displacement diagrams could be determined. While diameters up to 0.8 mm showed similar curves and thus a comparable material behaviour, deviations for particles with diameters of 1.0 mm occurred.

As Melentiev and Fang (2019) stated in their theoretical study on particle velocity in micro-abrasive jet machining, the kinetic energy of the particles as a decisive factor for plastic deformation is closely linked to the velocity. Thus, in present work, the particle velocities before and after the impact are analysed. The velocity reduction due to the impact depends on the material dependent amount of energy that is converted in the forming process. Therefore, the analysis of the velocities will provide information on the material properties. In their work, Melentiev and Fang further showed that not only the particle size and density but also the dimensions of the nozzles have a great influence on the flow conditions. The influence of the nozzle and the flow conditions must therefore be taken into account when interpreting the results of the presented work.

Remaining issues and motivation of the work presented here

Based on the research discussed above, the following open questions will be addressed in this work:

- Are descriptors evaluated in particle-oriented peening sensitive enough to distinguish between only slightly different heat treatment states of the same steel? What changes in material properties are reflected in the descriptors?

- Can we deduce information on the elasto-plastic material behaviour considering the velocities of the particles before and after the impact?

- Which conditions make a particle size independent comparison of the descriptors possible?

In order to gain first insights about the possible interrelationships with conventional material properties, the descriptors determined by particle-oriented peening are compared to the characteristic values obtained from universal micro hardness (UMH) measurements. As described in the review of this measuring method by Lucca et al. (2010) various elastic, elasto-plastic (e.g. the Martens hardness HM and the elastic deformation work W_{el}) and plastic properties (e.g. the indentation hardness H_{IT} and the plastic deformation work W_{pl}) can be derived from the instrumented indentation test. Identified correlations between the UMH and the quantities determined utilizing particle-oriented peening may replace conventional material testing in the future. Using short-term characterization methods like the particle-oriented peening, a fast determination of material properties is possible, enhancing the potential of application-oriented material development since testing cost and effort are significantly reduced.

2 Particle-oriented peening – Experimental setup

In order to process single particles, a new experimental setup is implemented. It consists of i) a separation unit in which the particles are separated and directed to the compressed air stream and ii) a process chamber in which the plastic deformation of the individual particles takes place (cf. Figure 1). The particles are conveyed by compressed air (white arrows) through a pneumatic hose towards the nozzle. By reducing the diameter of the hose down to the diameter of the nozzle opening, the particles are accelerated to process velocity. They hit the contact plate (hardened 100Cr6, 63 HRC). The impact force of the particles is measured by the aid of a piezoelectric dynamometer (manufactured by Kistler Instrumente GmbH) located under the contact plate. The deformed particles rebound and reach the aluminium cone underneath where

they exit the process chamber. Here, the particles are collected in the same order in which they were processed. Several windows have been designed in the housing to avoid a pressure increase inside the process chamber. A sieve mesh prevents particles from escaping.

For measuring the particle velocity, a system consisting of a light barrier (manufactured by "FOS Messtechnik GmbH"), two stroboscopes ("HELIO-STROB micro2" manufactured by "ELMED Messtechnik GmbH") and a monochrome camera (type "DMK 37BUX250" manufactured by "The Imaging Source Europe GmbH") is integrated into the experimental setup (cf. Figure 2). The stroboscopes provide a flash phase-shifted exposure with 2000 Hz each (total frequency = 4000 Hz). The light barrier activates the camera. In the recorded image, the particle appears several times during its approach and rebound due to the flash frequency and the shutter speed. Thus, it is possible to visualize the trajectory of a single particle by recording a single image and calculating its velocity before and after impact (cf. section 3.2).

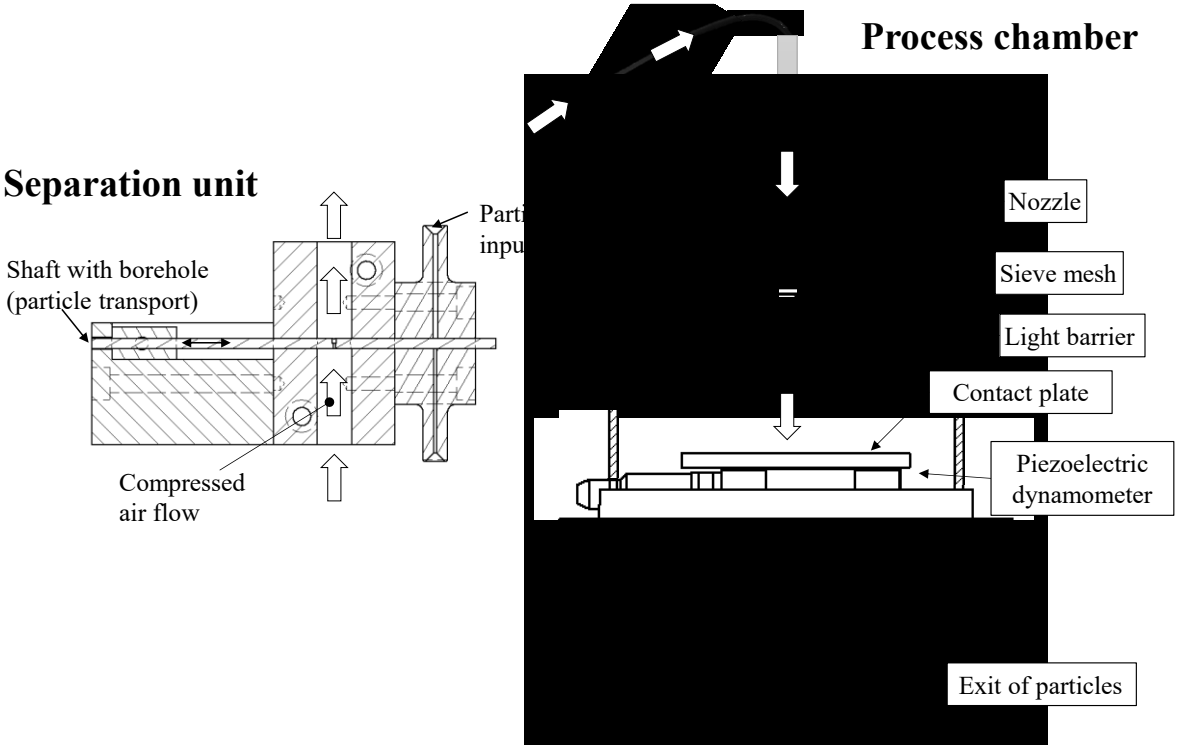

Figure 1 Scheme of the experimental setup (left: separation unit, right: process chamber); arrows indicate the trajectory of the particles due to the compressed air flow

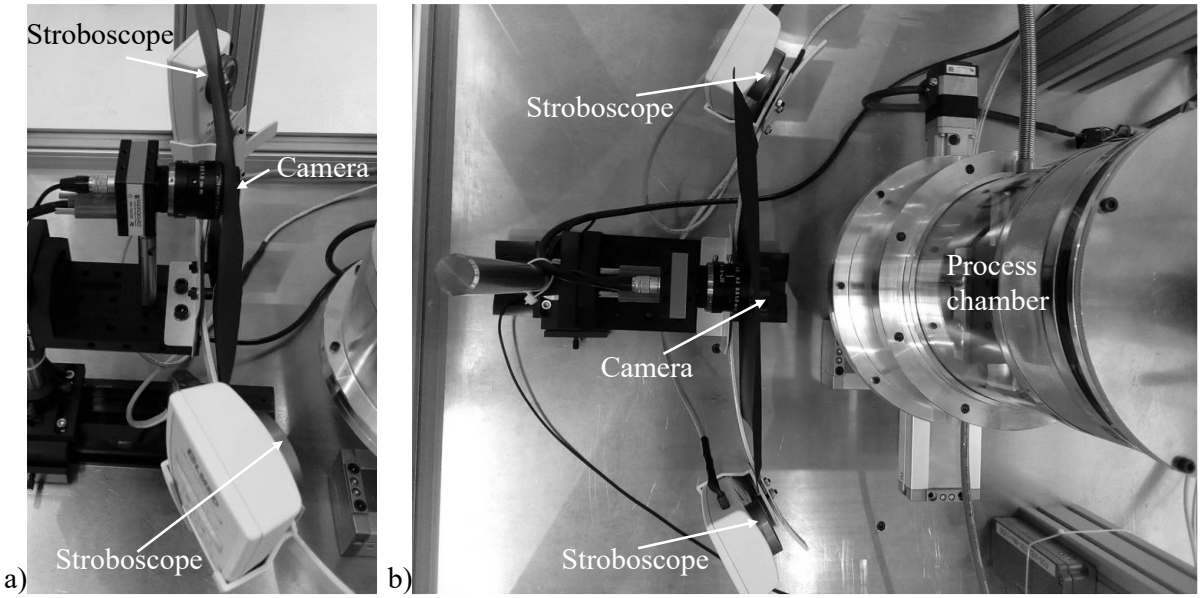

Figure 2 Set-up: speed measurement (a) side view, b) top view)

In order to analyse the process parameter dependent change of the descriptors evaluated in particle-oriented peening, the particles are accelerated using different jet pressures from 0.5 to 4.0 bar.

3 Characterization of micro particles

The particles analysed within this work are commercially available bearing balls with diameters of 0.6 mm (only for the 100Cr6-SA state cf. Table 1), 0.8 mm and 1.0 mm with a maximum deviation in size of ≤ 3 % each. The investigation of different diameters provides initial insights into the influence of particle size on the considered descriptors of the particle-oriented peening process. With the results of the diameter variation, scaling and normalization of the descriptors can be implemented. In order to investigate the influence of different heat treatments and especially the influence of different austenitizing temperatures, particles of the bearing steel 100Cr6 are investigated in three heat treatment states. To gain first insights into the influence of the alloy composition, X46Cr13 particles are additionally applied.

The heat treatment was performed according to the parameters in Table 1. The used abbreviations follow an internal project convention (SA ≙ soft annealed; Q ≙ quenched; QT ≙ quenched and tempered).

Table 1 Heat treatment of the investigated particles: 100Cr6 (AISI 52100) and X46CrC13 (AISI 420)

Material	Heat treatment	Hardening parameter	Quenching parameter	Tempering parameter
100Cr6	SA	600°C (30 min), 800°C (3 h), 690°C (3 h)	Oven cooling	-
100Cr6	Q800	800°C (1 h)	N_2 8 bar	-
100Cr6	Q1150	1150°C (10 min)	N_2 8 bar	-
X46Cr13	XQT	1050°C (1 h)	N_2 8 bar	N_2, 600°C (2h)

In Figure 3, microsections of the different heat treatment states are displayed. Regarding the 100Cr6-SA structure shown in Figure 3a), a bright ferrite matrix with homogeneously distributed, globularly moulded cementite can be identified. 100Cr6-Q800 (Figure 3b)) shows a fine-grained inter-stage structure (dark) with spherical chromium carbides (light). The comparatively low carbon content due to the low austenitizing temperature caused an increase in the critical quenching velocity. The microstructure contains only small amounts of martensite and no retained austenite. Figure 3c) shows the microstructure of the heat treatment variant 100Cr6-Q1150. Since more thermal energy was available due to the increased austenitizing temperature, grain coarsening occurred. The former austenite grain boundaries are pronounced by cementite. Martensite needles are clearly visible in the individual grains. The brighter structural areas can be identified as retained austenite. The microsection of X46Cr13 (Figure 3d)) shows a homogeneously quenched and tempered structure, i.e. tempered martensite with additional globular carbides (light) and small amounts of retained austenite. The microsections of 100Cr6-Q1150 and X46Cr13 show decarburization at the surface.

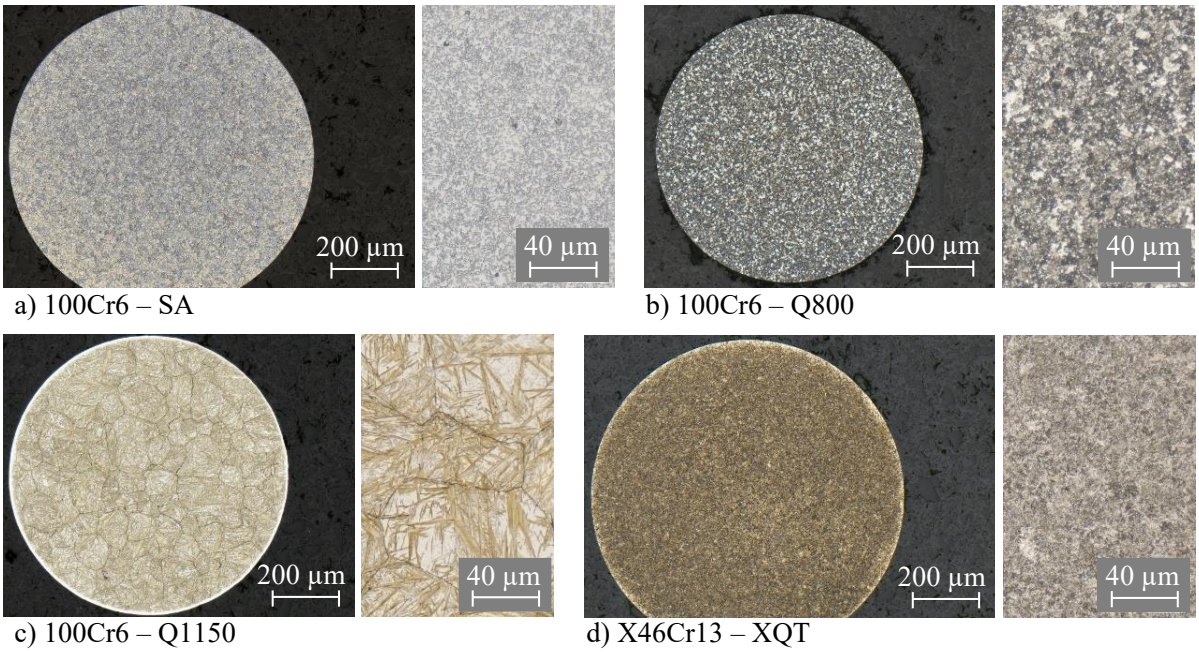

Figure 3 Microsections of embedded particles for the investigated material states

Within the investigations, it is assumed that the particles are ideally spherical and that after heat treatment in one batch, a similar, isotropic microstructure prevails. Since the spherical particles are introduced individually into the peening process, no further preparation after heat treatment is necessary.

3.1 Universal micro hardness measurements

In order to compare the material properties of the particles, instrumented universal micro hardness (UMH) measurements are performed using a testing device ("Fischerscope H100C") with a Vickers indenter. The particles are prepared by embedding and grinding to the equatorial plane. The ground surface of the embedded samples is polished subsequently. For UMH measurements, the largest particles processed within the present work (d_p = 1 mm) are used to reduce the influence of the embedding process and to allow the positioning of the indentations with standard-compliant distances according to DIN EN ISO 14577. A maximum indentation force of 1000 mN is used. The loading time, holding time and relief time are set to 10 s each. 25 measurements are performed on each particle, so that, with three (or more) particles of one heat treatment condition average values of at least 75 indentations can be used as statistical basis. The variables defined in Table 2 are obtained using UMH testing (cf. (Lucca et al., 2010)).

Table 2 Elasto-plastic material properties obtainable by performing micro hardness measurements (cf. (Lucca et al., 2010))

Variable	Symbol	Unit
Martens hardness	HM	[N/mm^2]
Indentation depth at maximum testing force	h_{max}	[µm]
Total deformation work	W_t	[µJ]
Elastic deformation work	W_{el}	[µJ]
Plastic deformation work	W_{pl}	[µJ]

Figure 4 shows the exemplary development of the indentation depth h as a function of the testing force F_t. The testing force is increased until the maximum force $F_{t,\,max}$ is reached. It is kept constant for 10 s before relief is granted. The indentation depth h_{max} is determined when the maximum test load is reached. The integral of the curve corresponds to the total deformation work W_t, which is divided into the plastic part W_{pl} (hatched) and the elastic part W_{el} (grey).

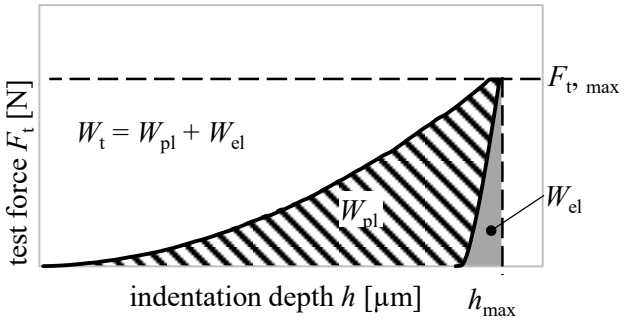

Figure 4 Exemplary trend of the indentation depth as a function of the testing force during a micro hardness measurement

3.2 Particle velocity

As described in the experimental setup (cf. section 2), the velocity measurement is based on the analysis of the recorded images for which the software Fiji (an extension of the java-based open source program ImageJ by Wayne Rasband) is used. Once calibrated with the help of a scale, the distances between two positions of the particle can be measured. At a known flash frequency, the velocity of the particle can be calculated. To examine the influence of the material state (alloy composition and heat treatment), the velocity of the particle before (v_1) and after impact (v_2) is taken into account. Figure 5 shows an exemplary image taken for a jet pressure of 2.5 bar and a nozzle distance of 80 mm for an X46Cr13 particle with a diameter of 1.0 mm.

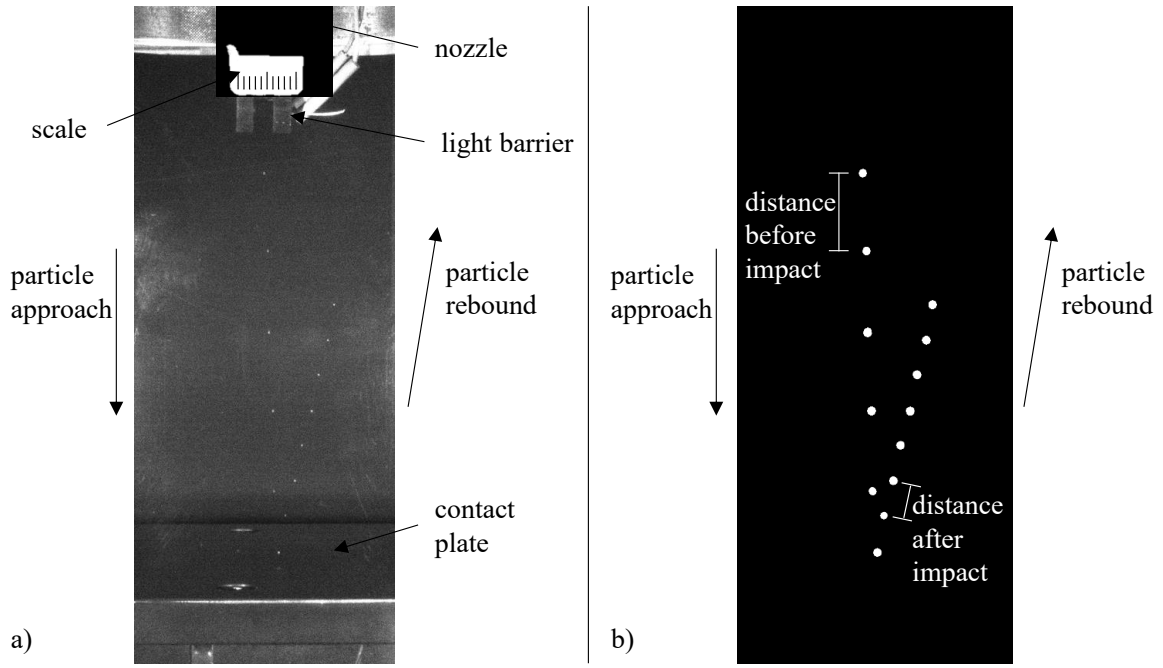

Figure 5 Image of the trajectory of an X46Cr13-XQT particle (d_p = 1.0 mm) accelerated with a jet pressure of 2.5 bar; a) camera image, b) contrast optimized image

The trajectory of the particle changes after the impact on the contact plate due to the flow of compressed air and particle rotation. However, the change of trajectory in direction of the orthogonal plane is negligible, since the deviations of the determined distances are small. As examined in a separate study, maximum angles between the particle approach and return are below 12° resulting in deviations of the determined rebound velocity of less than 2%.

3.3 Plastic deformation after particle-oriented peening

Despite the high accuracy of the particle size (max. size deviation ≤ 3 %), the exact radius of each particle is measured by optical microscopy before the experiment. The plastic deformation after the peening process is also determined individually for each particle using a Zeiss SteREO.V12 microscope.

After peening, the particles are plastically deformed and a flattened surface A_{def} occurs (cf. Figure 6). To measure the radius r_{def} of the flattened surface A_{def} with the microscope, the particles are manually positioned. The measured radius and surface are used to calculate the linear plastic deformation Δl and the volume of the deformed spherical segment V_{def}. The equations used to quantify the descriptors are based on the geometrical relations of a spherical segment (cf. Figure 6).

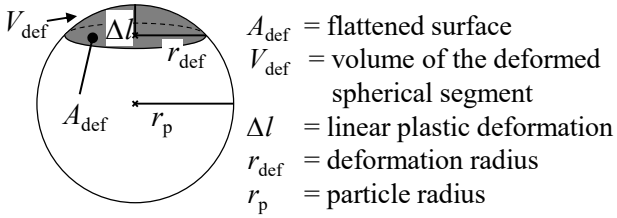

Figure 6 Sketch of a plastically deformed particle after shot peening with labels for the analysis of the deformation

3.4 Impact force

The piezoelectric dynamometer described in the experimental setup (cf. section 2) is used not only for process control but also for approximating the impact force *F*. As a result of previous calibration tests, a low pass filter of 3 kHz, a sampling rate of 100 kHz and the time constant DC-long are used for the measurements. Figure 7 illustrates the force measurement during the plastic deformation of a 100Cr6 particle (heat treatment: SA) with a diameter of 1.0 mm, which was accelerated with a jet pressure of 4 bar. The jet stream of compressed air leads to an increase in the basic level of the measured force which is comparable to a baseload of a measurement. The impact of the particle can be recognized by a pronounced peak in the force measurement. The base value due to the compressed air flow is subtracted from the maximum force value to determine the impact force. Due to the high dynamic of the peening process and the short contact time of the particle with the contact plate, the exact measurement of the impact force is not possible. But even though the dynamometer is not able to determine the actual impact force quantitatively, the extracted value still is sensitive to the particle size and peening parameter (e.g. jet pressure) and is therefore used as descriptor.

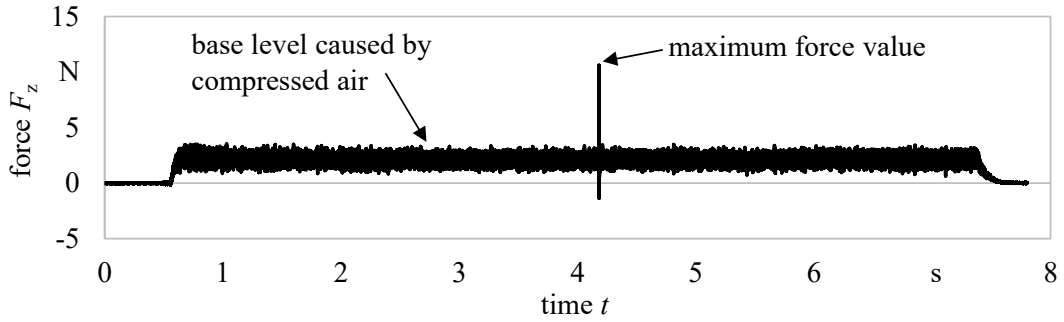

Figure 7 Exemplary force measurement of a 100Cr6 (SA) particle at a jet pressure p_s = 4 bar

4 Results and Discussion

4.1 Universal micro hardness measurements

Since the plastic deformation behaviour of the particles during the peening process is significantly dependent on their elasto-plastic properties, characteristic values of UMH measurements (cf. Table 3) are used for the interpretation of the results. According to the determined microstructure (cf. section 3), the highest plastic deformation for the 100Cr6 heat treatment states is expected for the SA condition. This expectation is supported by the UMH measurements since the lowest Martens hardness *HM*, the highest maximum indentation depth h_{max} and the maximum total deformation work W_t are reached for the 100Cr6-SA condition. With increasing austenitizing temperature from 100Cr6-Q800 to 100Cr6-Q1150 the Martens hardness increases, the maximum indentation depth and total deformation work decrease. Comparing all investigated material states, the highest plastic deformation work occurs at 100Cr6-SA. For X46Cr13-XQT and 100Cr6-Q800, the ratio of plastic and total deformation work (W_{pl}/W_t) is similar. The Martens hardness, the maximum indentation depth and the total deformation work determined for X46Cr13-XQT are in between the values determined for 100Cr6-Q800 and 100Cr6-Q1150.

Table 3 Elasto-plastic material properties obtained via UMH measurements of 100Cr6 and X46Cr13 depending on their heat treatment (± determined standard deviation)

	HM [N/mm^2]	h_{max} [µm]	W_t [µJ]	W_{el} [µJ]	W_{pl} [µJ]	W_{pl}/W_t [%]
100Cr6-SA	1737.31 ± 51.88	4.520 ± 0.069	1.537 ± 0.024	0.148 ± 0.003	1.389 ± 0.026	90.3 ± 0.3
100Cr6-Q800	3011.86 ± 106.22	3.423 ± 0.062	1.157 ± 0.019	0.185 ± 0.002	0.972 ± 0.022	84.0 ± 0.5
100Cr6-Q1150	5420.14 ± 249.81	2.539 ± 0.063	0.867 ± 0.021	0.264 ± 0.011	0.603 ± 0.029	69.5 ± 1.7
X46Cr13-XQT	3463.64 ± 43.80	3.189 ± 0.025	1.075 ± 0.005	0.179 ± 0.004	0.896 ± 0.001	83.3 ± 0.3

4.2 Particle velocity

One requirement for the comparability of different particle deformations due to an impact during the particle-oriented peening process is a constant approaching velocity of particles with similar volumes. Figure 8a) shows the development of the particle velocity with increasing jet pressure for the material state 100Cr6-SA. The mean values of at least three experiments are plotted for different particle sizes (d_p = 0.6 mm, d_p = 0.8 mm and d_p = 1.0 mm). The error bars represent the maximum and minimum values. With increasing jet pressure, an increase of the

determined particle velocity v_p before (v_1) and after the impact (v_2) is obtained for all particle sizes. The mass (resulting from the volume and the materials density) and the projected area of the spherical particles are taken as values to compare the different particle sizes. The approaching velocities of particles with a diameter of 0.8 mm and 1.0 mm are similar even though the mass of the bigger particles is about twice as large. The ratio of projected area and particle volume is similar for these diameters with values of 1.85 mm^2/mm^3 (d_p = 0.8 mm) and 1.5 (d_p = 1 mm). The approaching velocities of particles with a diameter of 0.6 mm are significantly lower than for the larger particles. Compared to particles with a diameter of 0.8 mm the mass of 0.6 mm particles is about 2.4 times smaller. The ratio of projected area and particle volume (2.5 mm^2/mm^3) differs significantly from the values obtained for the larger particles. The velocities below a jet pressure of 2 bar could not be determined for particles with a diameter of 0.6 mm since the light barrier was only triggered irregularly. Even if an image was recorded, a proper determination of the particle velocity was not always possible due to the small size of the reflection images generated by these particles. This measuring uncertainty is also reflected in the increase of deviation with increasing velocities for this particle size. Therefore, the number of experiments per jet pressure was increased for particles with a diameter of 0.6 mm to improve statistics. The velocities determined for the larger particles (d_p = 0.8 mm, d_p = 1.0 mm) are in the same order of magnitude. This can be explained by the geometric characteristics of the jet nozzle used. As mentioned in the introduction, the particle velocity is not only influenced by the density, mass, and geometry of the particle but also by the length and diameter of the nozzle. In this study, the nozzle diameter of 1.5 mm is only slightly (0.5 mm) bigger than the largest investigated particle diameter. As a result, the large particles are less likely to be surrounded by the flow but pushed forward. The flow changes to a plug flow and the effectiveness of the acceleration increases. This was already suspected by Kämmler et al. (2019), but could not be confirmed up to now due to the large number of simultaneously processed particles. The observation that, the velocity of the smallest particles differs significantly from the velocity of the larger ones confirms the assumption of a plug flow for the largest particle diameters. The influence of the nozzle geometry, as mentioned by Melentiev and Fang (2019), is thus reflected in the results. The correspondence in the order of magnitude of the determined velocities for the larger particles (d_p = 0.8 mm and d_p = 1.0 mm) was observed for all investigated material states. The approaching velocity is independent of the alloy composition and the heat treatment of the investigated materials. The mean value of the maximum approaching velocity of the particles with a diameter of 0.8 mm and 1.0 mm is

about 61 m/s and is shown in Figure 8b). Since the differences in density are small with 7.80 kg/dm^3 (100Cr6) and 7.85 kg/dm^3 (X46Cr13) the alloy composition does not significantly influence the approaching velocity.

The velocity of the particles is reduced after the impact due to the conversion of kinetic energy into plastic deformation. Although the particle velocities of all material states are similar for the approach phase, they significantly differ after the impact (Figure 8b)). The influence of the heat treatment is clearly visible. The higher the hardness of the particle (cf. Table 3), the higher is the rebound velocity. Despite the high deviation for the particles with a diameter of 0.8 mm of 100Cr6-Q800, the rebound velocity of this material state is similar to the rebound velocity of X46Cr13-XQT. Therefore, an identical hardness might be assumed.

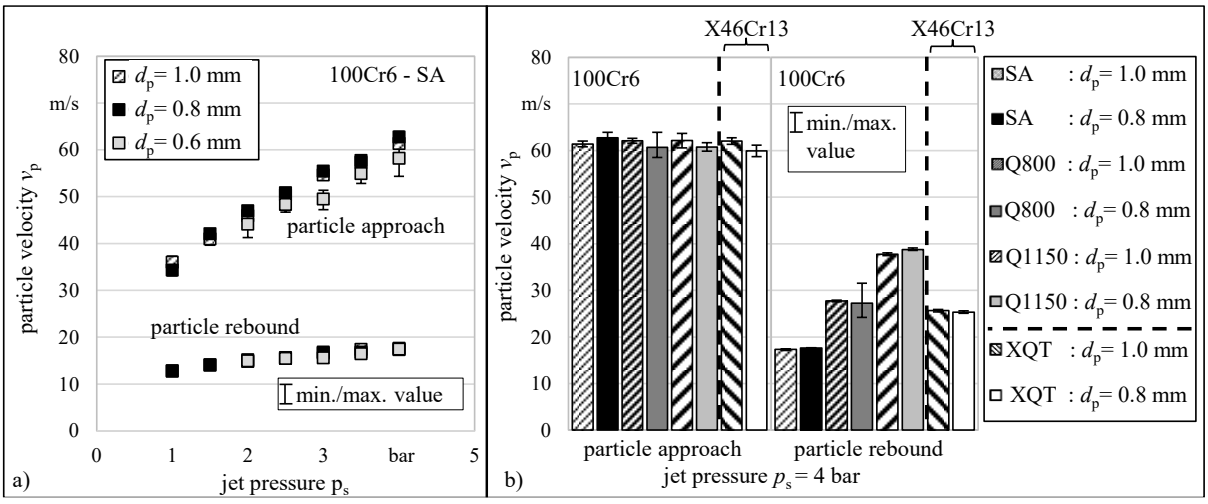

Figure 8 Particle velocity before (particle approach) and after (particle rebound) the impact a) for 100Cr6-SA at various jet pressures b) for all material states at a constant jet pressure of p_s = 4 bar (error bars indicate minimum and maximum values out of three measurements)

The percentage velocity reduction ($\Delta v_p = (1 - (v_2 / v_1)) \cdot 100\%$) and the respective standard deviation (σ) for a constant jet pressure of 4 bar (left) as well as the mean value of all investigated jet pressures (right) is presented in Table 4. At a constant jet pressure, standard deviations of the percentage velocity reduction for each particle size and for all material conditions are small with a maximum of $\sigma = \pm$ 3 %. Even for the mean value of all investigated jet pressures, for each material condition and particle size scattering is below 5 %. With increasing jet pressure, the velocity reduction approaches a maximum value. Hence, a characteristic percentage velocity reduction which is independent of the particle diameter but sensitive to material composition and heat treatment can be determined for each material condition. For the material states 100Cr6-Q800 and X46Cr13-XQT similar values can be determined (cf. Table 4; grey shaded).

Table 4 Percentage velocity reduction for each material state at a constant jet pressure of 4 bar and mean value for all jet pressures (σ = determined standard deviation)

	Jet pressure p_s = 4 bar		Mean of all jet pressures	
	Δv_p	σ	Δv_p	σ
100Cr6-SA / 1.0 mm	72%	0%	68%	2%
100Cr6-SA / 0.8 mm	72%	0%	68%	3%
100Cr6-SA / 0.6 mm	70 %	1%	69%	1%
100Cr6-Q800 / 1.0 mm	55%	1%	55%	3%
100Cr6-Q800 / 0.8 mm	55%	3%	52%	5%
100Cr6-Q1150 / 1.0 mm	39%	2%	39%	1%
100Cr6-Q1150 / 0.8 mm	36%	1%	33%	3%
X46Cr13-XQT / 1.0 mm	59%	0%	54%	3%
X46Cr13-XQT / 0.8 mm	58%	0%	53%	4%

In the range of the considered particle sizes and for the experimental set-up used, the mass has only a minor influence on the particle velocity (cf. Figure 8: d_p = 0.8 mm, 1.0 mm). Since the velocities before the impact are similar, a consideration of variations of the deformations caused by the impact is valid. Furthermore, the velocity is a quickly measurable descriptor, which is why in this first approach the comparison is based on matching particle velocities for all particle sizes. According to Figure 8, a jet pressure of 3 bar is required to accelerate a particle with a diameter of 0.6 mm to approximately 50 m/s. For larger particle sizes, this velocity is already reached at a jet pressure of 2.5 bar. A jet pressure of 3.5 bar is required for the smaller particles to achieve a particle velocity of 55 m/s. 4.0 bar is required for a particle velocity of 58 m/s (cf. Table 5). This offset of 0.5 bar seems to be linear in the considered velocity range and is therefore used for a better comparison of the particles with a diameter of 0.6 mm and the larger ones. The comparison is based on correlating velocities before the impact and is thus possible for the following parameter combinations:

Table 5 Jet pressures with similar particle velocities for a comparison of different particle sizes

d_b = 0.6 mm	
p_s [bar]	v_1 [m/s] ± σ
3.0	49.48 ± 1.21
3.5	54.94 ± 1.40
4.0	58.23 ± 1.79

	$d_b \geq 0.8$ mm	$d_b \geq 1.0$ mm
p_s [bar]	v_1 [m/s] ± σ	v_1 [m/s] ± σ
2.5	50.82 ± 0.95	50.40 ± 0.86
3.0	55.47 ± 1.29	54.64 ± 0.90
3.5	57.76 ± 1.02	57.30 ± 1.00

4.3 Plastic deformation

To analyse the plastic deformation after the particle-oriented peening process the radius of the deformed surface r_{def} is determined. Due to the dependency on the initial particle sizes, this value only allows a comparison of different material states for corresponding particle sizes.

Also, the calculated linear plastic deformation Δl, which was investigated by Kämmler et al. (2019), does not lead to the elimination of size dependencies. To enable a particle size independent material comparison or characterization, the deformation radius r_{def} is evaluated in relation to the initial particle radius r_p. The quotient of the two variables (r_{def}/r_p) in dependence of the jet pressure p_s is shown in Figure 9a) for all three particle sizes d_p of the 100Cr6-SA state. With increasing pressure, an increase in plastic deformation can be determined for all particle sizes. This increase approximately follows a logarithmic function (cf. Figure 9a: equations can be found in the boxes). A good agreement ($R^2 \geq 0.98$) is obtained for all curves. The plastic deformations of the particles with a diameter of 0.6 mm determined at a jet pressure of 2 bar and higher show higher deviations from those of larger particles. This corresponds to the lower particle velocities that were determined for the particles with a diameter of 0.6 mm in the previous section.

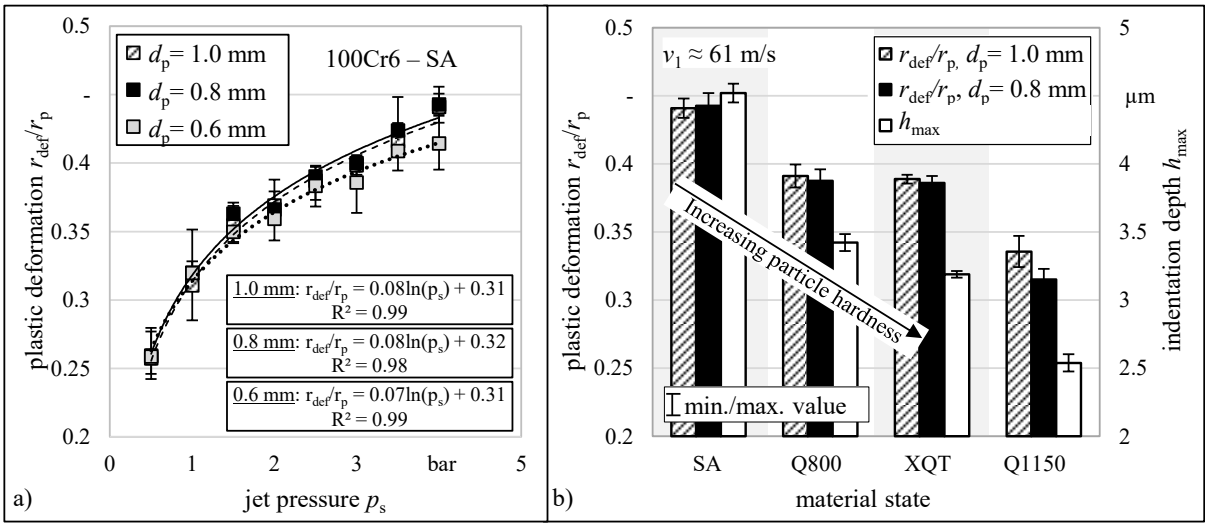

Figure 9 a) Plastic deformation r_{def}/r_p in dependence of jet pressure p_s and particle size d_p of 100Cr6 (SA); b) Visualization of the plastic deformation r_{def}/r_p (determined at a jet pressure of p_s = 4 bar) and the maximum indentation depth h_{max} for the investigated material states

Table 6 shows the plastic deformations (r_{def}/r_p) in dependence of the jet pressure. A comparison of the different particle sizes is possible for similar particle velocities before the impact according to Table 5. An offset of 0.5 bar regarding the particles with a diameter of 0.6 mm leads to similar plastic deformations. The consideration of the related plastic deformation as a descriptor is therefore reasonable, but only for comparable particle velocities or in relation to the particle velocity.

Table 6 Plastic deformations (r_{def}/r_p) determined for comparable particle velocities and different particle diameters

d_b = 0.6 mm	
p_s [bar]	r_{def}/r_p [-] ± σ
3.0	0.3856 ± 0.0075
3.5	0.4086 ± 0.0081
4.0	0.4143 ± 0.0095

	$d_b \geq 0.8$mm	$d_b \geq 1.0$mm
p_s [bar]	r_{def}/r_p [-] ± σ	r_{def}/r_p [-] ± σ
2.5	0.3901 ± 0.0042	0.3870 ± 0.0078
3.0	0.3999 ± 0.0042	0.3983 ± 0.0054
3.5	0.4238 ± 0.0132	0.4161 ± 0.0072

In Figure 9b) the plastic deformations determined for particles with a diameter of 0.8 mm and 1.0 mm of all investigated material states at a particle velocity of approximately 61 m/s (4 bar jet pressure) are compared to the maximum indentation depth h_{max} of UMH measurements (see secondary axis). For both, the plastic deformation (r_{def}/r_p) after particle-oriented peening and the maximum indentation depth of UMH measurements, as expected, a decrease can be observed with increasing material hardness. For the ductile material state 100Cr6-SA, the values determined for the plastic deformation and the maximum indentation depth differ by a factor of 10. This factor decreases with increasing material hardness. While the contact surface of the sample during UMH measurements is always even and polished, a geometrical effect caused by the particle curvature during contact in the peening process might have a higher influence on the results obtained for harder material states compared to experiments with more ductile material. Since the plastic deformation values and the corresponding velocity reductions determined for 100Cr6-Q800 and X46Cr13-XQT (cf. section 4.1) were similar, the same Martens hardness (and maximum indentation depth) is expected for both material states. In fact, even considering the high standard deviation, these two states differ in Martens hardness by over 300 N/mm². This indicates that the plastic deformation and further the material behaviour of the particles examined in the particle-oriented peening process cannot exclusively be approximated by the hardness, but that other variables must be taken into account. For the evaluation of the material states 100Cr6-Q800 and X46Cr13-XQT and for the interpretation of the corresponding plastic deformation despite different hardness, further quantities determined in the UMH are analysed in more detail. Although the total deformation work differs slightly, the plastic part of the total deformation work W_{pl}/W_t is about 83-84 % for both material states and thus in the same order of magnitude. This indicates that in addition to hardness, the plastic deformation work should also be considered when analysing the deformation behaviour. Figure 10 shows the relative plastic deformation work W_{pl}/W_t plotted over the plastic deformation r_{def}/r_p determined for particles with a diameter of 1.0 mm for corresponding particle velocities ($v_1 \approx 61$ m/s). For the investigated Fe-C-Cr-system a quadratic relationship

between the plotted quantities can be determined with a coefficient of determination of 0.99 (cf. Figure 10). This function approaches a relative plastic deformation of 91 % for high values of the plastic deformation.

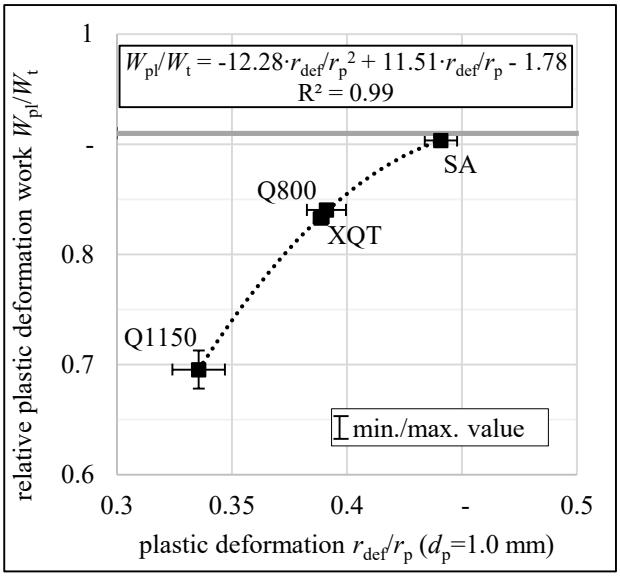

Figure 10 Relationship of the relative plastic deformation work W_{pl}/W_t (UMH) and the plastic deformation r_{def}/r_p (particle-oriented peening) determined for particles with a diameter of 1.0 mm for particle velocities of approx. 61 m/s

4.4 Impact force

The plastic deformation of the particles is significantly influenced by the impact force which in return depends on the jet pressure and the particle mass, i.e. the particle velocity. With increasing jet pressure, an increase of the determined impact force F is obtained as can be seen exemplarily for the material state 100Cr6-SA in Figure 11a). In addition to the absolute impact force values determined, the basic pressure levels of the air flow are additionally displayed in grey. The forces determined for the smallest diameter are in the same order of magnitude as the base levels, which makes a determination of the forces more difficult and error-prone. This is also reflected in the generally high deviations. For all particle sizes, the impact force is reaching a maximum value which is determined at the highest particle velocity. This is assumed to be due to air resistance, which counteracts further particle acceleration. The described behaviour can be observed for all investigated material states and approximately follows a logarithmic function shown for 100Cr6-SA in Figure 11c). When the particle diameter is reduced by 0.2 mm, a reduction of the slope of the logarithmic function by 46 % can be observed. This can be obtained for a diameter reduction from d_b = 1.0 mm to d_b = 0,8 mm and from d_b = 0.8 mm to d_b = 0.6 mm and corresponds to a mass reduction of about 49 % and 58 % respectively. The

influence of the mass is thus somehow reflected by the slope of the functions. Since the slope and mass reduction do only match for the larger particles, it can be assumed that with decreasing particle size, the influence of the mass decreases or further variables influence the determined impact force. It is possible that the backflow of air reduces the impact of small particles more distinctly. In the bar diagram in Figure 11b) the impact forces determined at a jet pressure of 4 bar with a particle velocity of approximately 61 m/s are displayed for each material state. The mean values of at least five measurements show a slight increase of the impact forces with increasing hardness (100Cr6; arrows). The values obtained for X46Cr13 fit into this observation. The error bars, which each represent the maximum and minimum value, show deviations up to 10 % for the 100Cr6 particles with a diameter of 1.0 mm. Even higher deviations occur for the 100Cr6 particles with a diameter of 0.8 mm reaching from 17 to 28 %. This result supports the assumption of a decreasing effect of the mass with decreasing particle diameter.

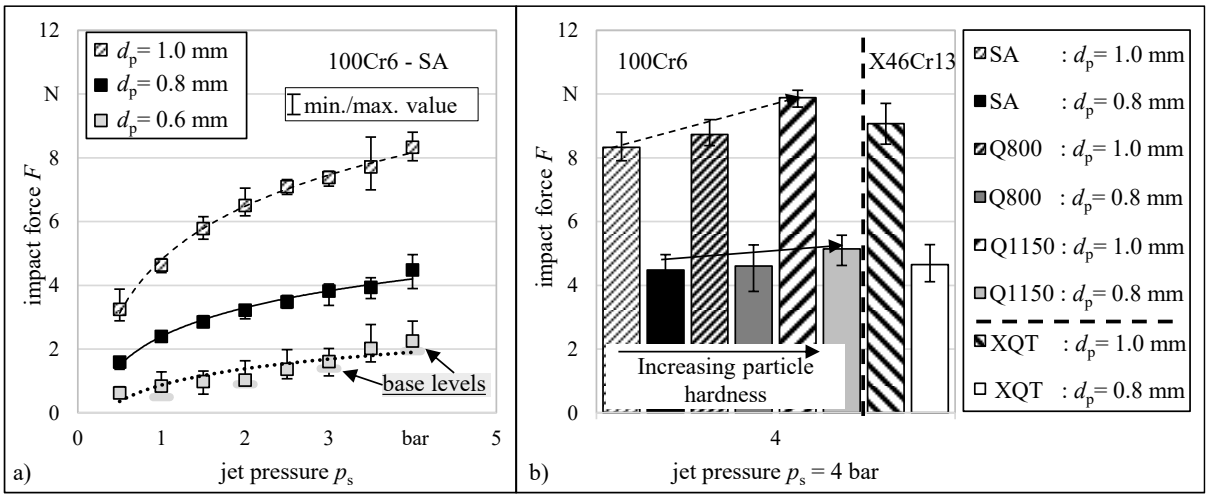

	Diameter	Functional relationship	Coefficient of determination
	d_p = 1.0 mm	$F = 2.4 \cdot \ln(p_s) + 4.8$	$R^2 = 0.99$
	d_p = 0.8 mm	$F = 1.3 \cdot \ln(p_s) + 2.4$	$R^2 = 0.98$
c)	d_p = 0.6 mm	$F = 0.7 \cdot \ln(p_s) + 0.9$	$R^2 = 0.81$

Figure 11 Impact forces determined for a) different jet pressures (100Cr6-SA) and b) various material states; c) Functional relationships of a) for various diameters

For a more detailed analysis of the relationship between the impact force and the hardness, the impact forces determined for various particle sizes are plotted over the Martens hardness in Figure 12. Since the particle velocity of 61 m/s could not be achieved for particles with a diameter of 0.6 mm, the values determined at 55 m/s are additionally shown (cf. Figure 12b). Thus, it is possible to evaluate the development of the conditions in dependence of the

approaching velocity. For both investigated velocities, linear relationships between the impact force and Martens hardness can be determined with a high coefficient of determination. For matching particle diameters, similar slopes of the functions can be observed. Only the y-axis intercept varies due to the different absolute values. The slope of the curves determined for particles with a diameter of 0.8 mm is 50% lower than the slope determined for particles with a diameter of 1.0 mm. This value is in the same order of magnitude as the mass reduction. The impact force determined for particles with a diameter of 0.6 mm for the condition 1000Cr6-SA is additionally plotted in Figure 12b. It shows a reduction of 50 % of the value determined for particles with a diameter of 0.8 mm. A similar functional relationship between the impact force and the Martens hardness for the small particle size seems possible. It can be stated that the influence of the particle size can be determined by the used measuring setup and that different heat treatments can be distinguished regarding the values determined for the impact force.

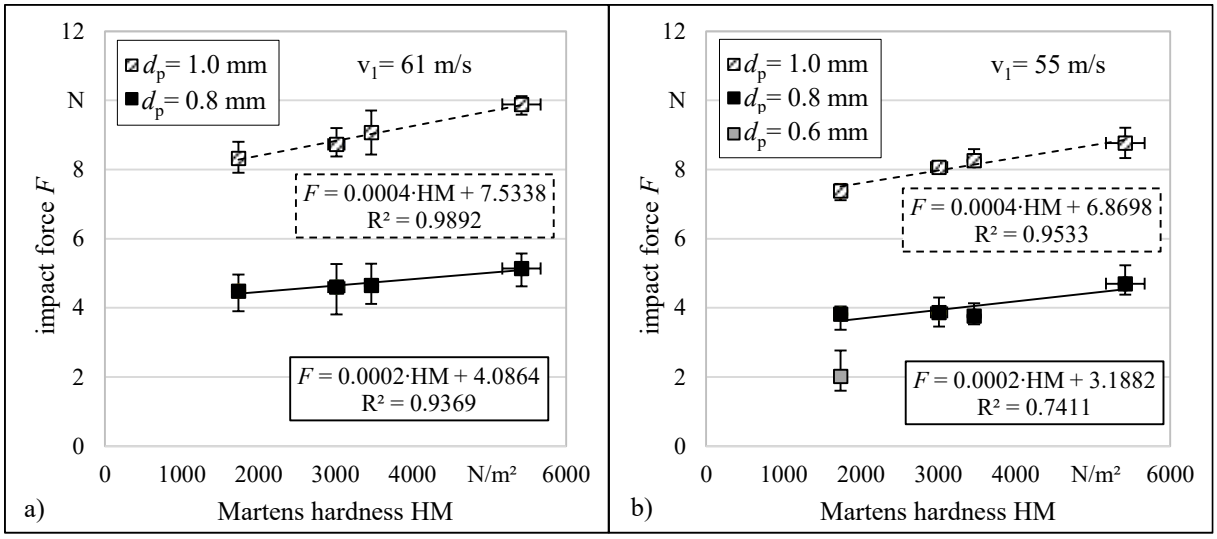

Figure 12 Impact forces determined for various particles sizes with approach velocities of a) 61 m/s and b) 55 m/s in relation to the Martens hardness

Since the particles with identical masses were accelerated to similar velocities and thus have the same impulse ($p = m_p \cdot v_1$), it seems contradictory that this distinction is possible. A higher maximum force can only be obtained if the contact time (i.e. the time in which deformation occurs) also changes with a change in hardness ($F = p / t_c$). Since the time of contact is not measurable with the current measuring setup, it is estimated utilizing the following equation of uniformly accelerated movement (assuming that the particle is uniformly decelerated during the contact).

$$\Delta l = -\frac{1}{2} \cdot a_p \cdot {t_c}^2 = -\frac{1}{2} \cdot \left(-\frac{v_1}{t_c}\right) \cdot t_c^2 \qquad \rightarrow t_c = 2 \cdot \frac{\Delta l}{v_1}$$

The contact times calculated for the investigated material states are listed in Table 7. The calculation is based on Δl determined for the particles with a diameter of 1 mm after particle-oriented peening with a particle velocity of approx. 61 m/s. The highest contact time was calculated for the softest material condition (100Cr6-SA). With increasing hardness, the contact time tends to decrease, which can be seen in the lower values calculated for the other material states. Despite different hardness (cf. Table 3), similar values result for 100Cr6-Q800 and X46Cr13-XQT. These observations support the hypothesis presented above: If the maximum force is calculated as the quotient of impulse and contact time, higher maximum forces can be determined for harder material states due to the decrease in contact time with increasing hardness.

Table 7 Calculated contact times t_c for all investigated material states

	$t_c \pm \sigma$ [µs]
100Cr6-SA	1.69 ± 0.05
100Cr6-Q800	1.31 ± 0.06
100Cr6-Q1150	0.95 ± 0.07
X46Cr13-XQT	1.29 ± 0.02

The functional relationships found within the investigated Fe-C-Cr alloy system theoretically allow the calculation of the material hardness based on a measured impact force. Due to the high deviation of the determined impact forces this calculated hardness should only be considered in combination with other variables.

5 Conclusions

In the present work, several descriptors derived from particle-oriented peening are introduced. The particle velocity, the plastic deformation, and the impact force are derived during and after the process as characteristic values. The aim of this work was to analyze the sensitivity of those descriptors to changes in material properties due to material composition or heat treatment. Major new findings of this work are:

- The velocity reduction Δv_p as well as the plastic deformation r_{def}/r_p were identified as useful normalized descriptors which are independent of the particle diameter but sensitive to the material composition and the heat treatment. In combination they allow statements on both, plastic and elastic material behaviour.

- The impact force F can be correlated with material hardness since the maximum force value is influenced by the impulse and the contact time.
- A functional correlation between the relative plastic deformation work W_{pl}/W_t (UMH) and the plastic deformation examined in a particle-oriented peening process was identified for the investigated Fe-C-Cr alloy system. This suggests that after calibration by UMH measurements, particle-oriented peening could be utilized for a faster characterization of new materials in the future.

Acknowledgements

Financial support of the subprojects U04 ‘Mechanical Treatment’ and D01 ‘Qualification of Material Conditions with Mechanical and Physical–Measuring Methods’ of the CRC 1232 “Farbige Zustände” funded by the Deutsche Forschungsgemeinschaft (DFG, German Research Foundation) – Projektnummer 276397488 – SFB 1232 is gratefully acknowledged.

References

Antonyuk, S., 2006. Deformations- und Bruchverhalten von kugelförmigen Granulaten bei Druck- und Stoßbeanspruchung, docupoint-Verl., Magdeburg.

Ellendt, N., Ciftci, N., Goodreau, C., Uhlenwinkel, V., Mädler, L., 2016. Solidification of single droplets under combined cooling conditions. IOP Conf. Ser.: Mater. Sci. Eng., vol. 117, 12057.

Ellendt, N., Mädler, L., 2018. High- troughput Exploration of Evolutionary Structural Materials. HTM, 175–186.

Imani Moqadam, S., Baune, M., Bösing, I., Heinzel, C., Meyer, D., Thomann, A., Wielki, N., Ellendt, N., 2020. Reproducibility of High-Throughput Sample Properties Produced by a High-Temperature Molten Metal Droplet Generator. Metals, vol. 10, 297.

Imani Moqadam, S., Mädler, L., Ellendt, N., 2019. A High Temperature Drop-On-Demand Droplet Generator for Metallic Melts. Micromachines, vol. 10.

Kämmler, J., Wielki, N., Guba, N., Ellendt, N., Meyer, D., 2019. Shot peening using spherical micro specimens generated in high-throughput processes. Mat.-wiss. u. Werkstofftech., vol. 50, 5–13.

Lucca, D.A, Herrmann, K., Klopfstein, M.J, 2010. Nanoindentation. Measuring methods and applications. CIRP Annals, vol. 59, 803–819.

Mädler, L., 2014. Is High-throughput screening for structural materials/metals possible?, Proceedings of the 4th International Conference on Nanomanufacturing (nanoMan2014), Bremen.

Melentiev, R., Fang, F., 2019. Theoretical study on particle velocity in micro-abrasive jet machining. Powder Technology, vol. 344, 121–132.

Schulze, V., 2006. Modern mechanical surface treatment. States, stability, effects, Wiley-VCH Verl., Weinheim.

Sonnenberg, H., Clausen, B., 2018. Mikrodruckprüfung an sphärischen Proben. Compression tests on spherical micro samples. In: G. Moninger (Ed.), Tagungsband Werkstoffprüfung 2018, Bad-Neuenahr, Deutschland, pp. 143–148.

Steinbacher, M., Alexe, G., Baune, M., Bobrov, I., Bösing, I., Clausen, B., Czotscher, T., Epp, J., Fischer, A., Langstädtler, L., Meyer, D., Raj Menon, S., Riemer, O., Sonnenberg, H., Thomann, A., Toenjes, A., Vollertsen, F., Wielki, N., Ellendt, N., 2019. Descriptors for High Throughput in Structural Materials Development. High-Throughput, vol. 8, 22.

Thelning, K.E. (Ed.), 2013. Steel and its heat treatment, Butterworth-Heinemann, Oxford.

Zhao, J.-C., 2006. Combinatorial approaches as effective tools in the study of phase diagrams and composition–structure–property relationships. Prog. Mater. Sci., vol. 51, 557–631.

Figures

Figure 1 Scheme of the experimental setup (left: separation unit, right: process chamber); arrows indicate the trajectory of the particles due to the compressed air flow

Figure 2 Set-up: speed measurement (a) side view, b) top view)

Figure 3 Microsections of embedded particles for the investigated material states

Figure 4 Exemplary trend of the indentation depth as a function of the testing force during a micro hardness measurement

Figure 5 Image of the trajectory of an X46Cr13-XQT particle (d_p = 1.0 mm) accelerated with a jet pressure of 2.5 bar; a) camera image, b) contrast optimized image

Figure 6 Sketch of a plastically deformed particle after shot peening with labels for the analysis of the deformation

Figure 7 Exemplary force measurement 100Cr6 (SA) particle at a jet pressure p_s = 4 bar

Figure 8 Particle velocity before (particle approach) and after (particle rebound) the impact a) for 100Cr6-SA at various jet pressures b) for all material states at a constant jet pressure of p_s = 4 bar (error bars indicate minimum and maximum values out of three measurements)

Figure 9 a) Plastic deformation r_{def}/r_p in dependence of jet pressure p_s and particle size d_p of 100Cr6 (SA); b) Visualization of the plastic deformation r_{def}/r_p (determined at a jet pressure of p_s = 4 bar) and the maximum indentation depth h_{max} for the investigated material states

Figure 10 Relationship of the relative plastic deformation work W_{pl}/W_t (UMH) and the plastic deformation r_{def}/r_p (particle-oriented peening) determined for particles with a diameter of 1.0 mm for particle velocities of approx. 61 m/s

Figure 11 Impact forces determined for a) different jet pressures (100Cr6-SA) and b) various material states; c) Functional relationships of a) for various diameters

Figure 12 Impact forces determined for various particles sizes with approach velocities of a) 61 m/s and b) 55 m/s in relation to the Martens hardness

Tables

Table 1 Heat treatment of the investigated particles: 100Cr6 (AISI 52100) and X46CrC13 (AISI 420)

Table 2 Elasto-plastic material properties obtainable by performing micro hardness measurements (cf. (Lucca et al., 2010))

Table 3 Elasto-plastic material properties obtained via UMH measurements of 100Cr6 and X46Cr13 depending on their heat treatment (± determined standard deviation)

Table 4 Percentage velocity reduction for each material state at a constant jet pressure of 4 bar and mean value for all jet pressures (σ = determined standard deviation)

Table 5 Jet pressures with similar particle velocities for a comparison of different particle sizes

Table 6 Plastic deformations (r_{def}/r_p) determined for comparable particle velocities and different particle diameters

Table 7 Calculated contact times t_c for all investigated material states

---

Author Contributions

Nicole Wielki performed and analysed the particle-oriented peening experiments and wrote the paper by the aid of Heike Sonnenberg, who performed microhardness measurements. Daniel Meyer and Brigitte Clausen supervised all investigations and supported with their expert knowledge. The CRC 1232 ‘Farbige Zustände’ contributed the investigated materials.

Declaration of interests

☒ The authors declare that they have no known competing financial interests or personal relationships that could have appeared to influence the work reported in this paper.